Article

NMR Hyperfine Shifts in Blue Copper Proteins: A Quantum Chemical Investigation

Yong Zhang, and Eric Oldfield

J. Am. Chem. Soc., **2008**, 130 (12), 3814-3823 • DOI: 10.1021/ja075978b

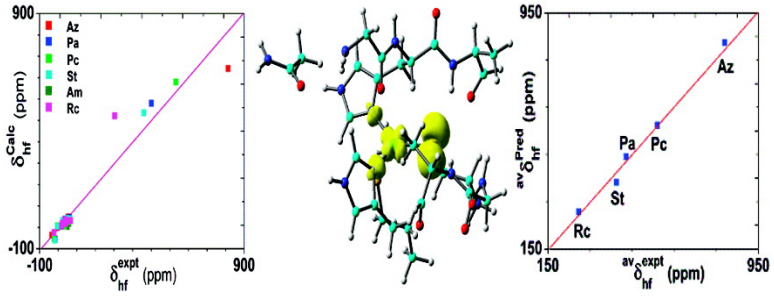

More About This Article

Additional resources and features associated with this article are available within the HTML version:

- Supporting Information
- Access to high resolution figures
- Links to articles and content related to this article
- Copyright permission to reproduce figures and/or text from this article

View the Full Text HTML

J|A|C|S
ARTICLES
Published on Web 03/04/2008

NMR Hyperfine Shifts in Blue Copper Proteins: A Quantum Chemical Investigation

Yong Zhang[†,‡] and Eric Oldfield*[,†]

Department of Chemistry, University of Illinois at Urbana−Champaign, 600 South Mathews Avenue, Urbana, Illinois 61801 and Department of Chemistry and Biochemistry, University of Southern Mississippi, 118 College Drive #5043, Hattiesburg, Mississippi 39406

Received August 8, 2007; E-mail: eo@chad.scs.uiuc.edu

Abstract: We present the results of the first quantum chemical investigations of ^{1}H NMR hyperfine shifts in the blue copper proteins (BCPs): amicyanin, azurin, pseudoazurin, plastocyanin, stellacyanin, and rusticyanin. We find that very large structural models that incorporate extensive hydrogen bond networks, as well as geometry optimization, are required to reproduce the experimental NMR hyperfine shift results, the best theory vs experiment predictions having $R^2 = 0.94$, a slope = 1.01, and a SD = 40.5 ppm (or ∼4.7% of the overall ∼860 ppm shift range). We also find interesting correlations between the hyperfine shifts and the bond and ring critical point properties computed using atoms-in-molecules theory, in addition to finding that hyperfine shifts can be well-predicted by using an empirical model, based on the geometry-optimized structures, which in the future should be of use in structure refinement.

Introduction

The NMR shifts of paramagnetic metal−ion-containing systems can provide interesting information about structure,[1,2] and NMR has been used for many years in investigating, in particular, the structures of paramagnetic metalloproteins.[3,4] For example, the iron centers in paramagnetic proteins (and model systems) have a >5000 ppm range of ^{13}C NMR shifts[5,6] and are well-correlated with electronic structure.[7] While ^{1}H NMR shifts are typically smaller, recent studies on several blue copper proteins (BCPs), amicyanin (Am),[8] azurin (Az),[9] plastocyanin (Pc),[10] pseudoazurin (Pa),[11] stellacyanin (St),[9] and rusticyanin (Rc),[11] revealed that the Cys−C$^\beta$H$_2$ shifts are in the range of ∼240−850 ppm,[9−11] since they are only three bonds removed from the paramagnetic (Cu^{II}) center. Such a large shift range strongly suggests that ^{1}H NMR spectroscopy should be a useful technique with which to probe the active site structures of these and other copper-containing proteins. To date, there have been no reports of the quantum chemical investigation of NMR hyperfine shifts in BCPs.

In general, hyperfine shifts (as well as chemical shifts) in proteins are difficult to compute accurately, since uncertainties in the X-ray coordinates[12] are usually much larger than in small molecule structures. In addition, for ^{1}H NMR shifts, the atoms of interest (hydrogens) are not even "seen" in protein X-ray structures, which obviously exacerbates the problem of predicting their shifts. Here, we thus explore the question of how to accurately predict ^{1}H NMR hyperfine shifts in BCPs, using large structural models. We find that these hyperfine shifts can be quite accurately predicted and that there are numerous interesting correlations between the hyperfine shifts (spin densities) and a variety of geometric factors, as well as bond and ring critical point properties, calculated by using atoms-in-molecules (AIM) theory.[13,14]

Computational Details

The experimentally observed NMR "chemical" shift (δ_{obs}) includes both a diamagnetic and an orbital contribution (δ_{dia}), from paired electrons, and a hyperfine contribution (δ_{hf}), from unpaired electrons:[7,15−17]

[†] University of Illinois.
[‡] University of Southern Mississippi.

(1) La Mar, G. N. In *NMR of Paramagnetic Molecules, Principles and Applications*; La Mar, G. N., Horrocks, W. D., Jr., Holm, R. H., Eds.; Academic Press: New York, 1973; pp 86−127.
(2) Walker, F. A. In *The Porphyrin Handbook*; Kadish, K. M., Smith, K. M., Guilard, R., Eds.; Academic Press: San Diego, 2000; Vol. 5, pp 81−184.
(3) Iwahara, J.; Clore, G. M. *Nature* **2006**, *440*, 1227−1230.
(4) Hansen, D. F.; Led, J. J. *Proc. Natl. Acad. Sci. U.S.A.* **2006**, *103*, 1738−1743.
(5) Goff, H. M.; Shimomura, E. T.; Phillippi, M. A. *Inorg. Chem.* **1983**, *22*, 66−71.
(6) Fujii, H. *J. Am. Chem. Soc.* **2002**, *124*, 5936−5937.
(7) Mao, J. H.; Zhang, Y.; Oldfield, E. *J. Am. Chem. Soc.* **2002**, *124*, 13911−13920.
(8) Kalverda, A. P.; Salgado, J.; Dennison, C.; Canters, G. W. *Biochemistry* **1996**, *35*, 3085−3092.
(9) Bertini, I.; Fernandez, C. O.; Karlsson, B. G.; Leckner, J.; Luchinat, C.; Malmstrom, B. G.; Nersissian, A. M.; Pierattelli, R.; Shipp, E.; Valentine, J. S.; Vila, A. J. *J. Am. Chem. Soc.* **2000**, *122*, 3701−3707.
(10) Bertini, I.; Ciurli, S.; Dikiy, A.; Gasanov, R.; Luchinat, C.; Martini, G.; Safarov, N. *J. Am. Chem. Soc.* **1999**, *121*, 2037−2046.
(11) Donaire, A.; Jimenez, B.; Fernandez, C. O.; Pierattelli, R.; Niizeki, T.; Moratal, J. M.; Hall, J. F.; Kohzuma, T.; Hasnain, S. S.; Vila, A. J. *J. Am. Chem. Soc.* **2002**, *124*, 13698−13708.
(12) Ray, G. B.; Li, X. Y.; Ibers, J. A.; Sessler, J. L.; Spiro, T. G. *J. Am. Chem. Soc.* **1994**, *116*, 162−176.
(13) Bader, R. F. W. *Atoms in Molecules—A Quantum Theory*; Oxford University Press: Oxford, 1990.
(14) Bader, R. F. W. *J. Phys. Chem. A* **1998**, *102*, 7314−7323.
(15) Wilkens, S. J.; Xia, B.; Weinhold, F.; Markley, J. L.; Westler, W. M. *J. Am. Chem. Soc.* **1998**, *120*, 4806−4814.
(16) Zhang, Y.; Sun, H. H.; Oldfield, E. *J. Am. Chem. Soc.* **2005**, *127*, 3652−3653.
(17) Kervern, G.; Pintacuda, G.; Zhang, Y.; Oldfield, E.; Roukoss, C.; Kuntz, E.; Herdtweck, E.; Basset, J. M.; Cadars, S.; Lesage, A.; Coperet, C.; Emsley, L. *J. Am. Chem. Soc.* **2006**, *128*, 13545−13552.

10.1021/ja075978b CCC: $40.75

$$\delta_{obs} = \delta_{dia} + \delta_{hf} \quad (1)$$

and the hyperfine shift can be further broken down into Fermi contact (δ_{FC}) and pseudocontact (δ_{pc}) terms:

$$\delta_{hf} = \delta_{FC} + \delta_{pc} \quad (2)$$

The δ_{FC} of a given nucleus depends on the spin state (S) of the system, the spin density at the nucleus ($\rho_{\alpha\beta}$), and the temperature (T):[7]

$$\delta_{FC} = m(S+1)\rho_{\alpha\beta}/T \quad (3)$$

where m is a collection of physical constants and is equal to 2.35×10^7 ppm K au^{-1}.[7] The δ_{pc} contribution is typically very small when compared with δ_{FC}, as discussed previously,[7,15−17] so in general, δ_{FC} dominates the hyperfine shift.

To calculate the NMR hyperfine shifts in BCPs, we used the hybrid Hartree−Fock/density functional theory method, B3LYP,[18] together with a Wachters' basis set (without the f functions) for Cu,[19,20] a 6-311G* basis for all other heavy (C, N, O, and S) atoms and 6-31G* for hydrogens, as implemented in Gaussian 03.[21] This is basically the approach that we used previously to evaluate both solution and solid-state NMR hyperfine shifts, as well as other hyperfine (ESR, ENDOR) properties.[7,16,17,22] Spin densities were converted to hyperfine shifts by using the relation obtained previously:[7]

$$\delta_{hf} = 1.89 \times 10^7 (S+1)\rho_{\alpha\beta}/T - 3.2 \quad (4)$$

The X-ray structure of each protein was used as a starting structure from which we constructed various computational models, probing the effects of different structural features on the hyperfine shift predictions. The Protein Data Bank (PDB) structure file numbers and their corresponding crystallographic resolutions were as follows: 1AAC (1.31 Å) for Am;[23] 1NWP (1.60 Å) for Az;[24] 1PLC (1.33 Å) for Pc;[25] 1BQK (1.35 Å) for Pa;[26] 1JER (1.60 Å) for St;[27] and 2CAK (1.27 Å) for Rc.[28] These are generally the highest resolution structures for these proteins, except for Am and Az, where two new higher resolution structures (i.e., 2OV0, 0.75 Å;[29] 2CCW, 1.13 Å;[30] respectively) were recently deposited in the PDB and were also investigated for comparison. We also investigated 4AZU (1.90 Å)[31] for Az, to address the possible effects of species differences on the NMR hyperfine shift predictions. For Rc, 1RCY[32] (1.90 Å) was also used to investigate an alternative hydrogen-bonding pattern involving the His ligand, as compared to that seen in the 2CAK structure. In each of the protein X-ray structures used in the calculations, hydrogen positions were set to standard values: $R_{CH} = 1.09$ Å and $R_{NH} = 1.01$ Å.

To investigate the effects of different structural units on the shift calculations, we used eight sets of structural models. The minimal structural model (Calc1) contained the strong equatorial ligands, His, His, and Cys (common to each of the BCPs studied), and the X-ray geometries were utilized without any optimization. This approach was used in previous computational studies of ESR hyperfine couplings in Az.[33] However, in our calculations, complete amino acids were used, rather than imidazole (for His) and SCH_3 (for Cys).[33] In a second set of calculations (Calc2), partial geometry optimization of Cu and the Cys SCH_2 moiety in the Calc1 structures was performed. To evaluate the effects on spin density from other structural units, including the weak axial ligands and hydrogen-bonded partners, we carried out six additional sets of calculations (Calc3−Calc8) using larger models, incorporating each of the residues listed in Table S1 in the Supporting Information. The Calc3 model used the experimental X-ray coordinates (as in the Calc1 model); however, in addition to Cu and the three equatorial ligands included in the Calc1 and Calc2 models, we included the axial ligand (Met/Gln) together with a conserved Asn (in Am, Az, Pc, Pa, and St; Ser in Rc) residue (next to the N-terminal His), which forms a H-bond with Cys.[34] This Calc3 model is basically of the same size as the largest QM model used in recent ab initio calculations on Pc,[35,36] in which the Asn residue was found to have significant influence on spin densities. In the Calc3 model for Az, the Gly residue in the fifth coordination position (trans to the axial Met ligand) was also included because of its short distance to Cu. Overall, the Calc3 models consist of ≥80 atoms. The Calc4 models differ from the Calc3 models in that the Cys SCH_2 moiety was geometry optimized. In the Calc5 model, Cu was also included in the optimization. In the Calc6 model, we also included the residue before the N-terminal His, for BCPs other than Az (for Az, this residue was already included in the Calc3 model). In Am, Pc, Pa, and St, this residue has a carbonyl oxygen of the peptide bond positioned in the fifth coordination position (trans to the axial Met/Gln ligand) and was found to have some effects on calculated reduction potentials.[37] The geometries of all first-coordination sphere atoms were optimized in these Calc6 models. The largest models in our work, Calc7 and Calc8, were designed to include all residues that are hydrogen bonded to the Cu ligands including those with Cys.[38−42] These Calc7 and Calc8 models are even larger than those reported recently[37,43] since the hydrogen bond partners to His ligands are included. The use of complete Cu ligands, their hydrogen bond partners, geometry optimization of the Cys SCH_2 moiety plus Cu, and all its coordinated atoms (the Calc7 models) was found to be necessary to reproduce the experimental NMR hyperfine shifts. For purposes of comparison, we also carried out a series of calculations (Calc 8) that had the same size as the Calc7 models but where no geometry optimizations were performed. The exact residues in each of the structural models are listed in Table S1, with the largest models including up to 10 residues. In the case of Rc, the only BCP studied here that has two possible hydrogen-bonding patterns for the N-terminal His ligand, a Calc9 model was also used, in which the whole His ligand

(18) Becke, A. D. *J. Chem. Phys.* **1993**, *98*, 5648−5652.
(19) Wachters, A. J. *J. Chem. Phys.* **1970**, *52*, 1033−1036.
(20) http://www.emsl.pnl.gov/forms/basisform.html.
(21) Frisch, M. J., et al. *Gaussian 03*, Revision B.03; Gaussian, Inc.: Pittsburgh, PA, 2003.
(22) Zhang, Y.; Gossman, W.; Oldfield, E. *J. Am. Chem. Soc.* **2003**, *125*, 16387−16396.
(23) Cunane, L. M.; Chen, Z. W.; Durley, R. C. E.; Mathews, F. S. *Acta Crystallogr. D* **1996**, *52*, 676−686.
(24) Chen, Z. W.; Barber, M. J.; McIntire, W. S.; Mathews, F. S. *Acta Crystallogr. D* **1998**, *54*, 253−268.
(25) Guss, J. M.; Bartunik, H. D.; Freeman, H. C. *Acta Crystallogr. B* **1992**, *48*, 790−811.
(26) Inoue, T.; Nishio, N.; Suzuki, S.; Kataoka, K.; Kohzuma, T.; Kai, Y. *J. Biol. Chem.* **1999**, *274*, 17845−17852.
(27) Hart, P. J.; Nersissian, A. M.; Herrmann, R. G.; Nalbandyan, R. M.; Valentine, J. S.; Eisenberg, D. *Protein Sci.* **1996**, *5*, 2175−2183.
(28) Barrett, M. L.; Harvey, I.; Sundararajan, M.; Surendran, R.; Hall, J. F.; Ellis, M. J.; Hough, M. A.; Strange, R. W.; Hillier, I. H.; Hasnain, S. S. *Biochemistry* **2006**, *45*, 2927−2939.
(29) Carrell, C. J.; Davidson, V. L.; Chen, Z.; Cunane, L. M.; Trickey, P.; Mathews, F. S. To be published.
(30) Paraskevopoulos, K.; Sundararajan, M.; Surendran, R.; Hough, M. A.; Eady, R. R.; Hillier, I. H.; Hasnain, S. S. *Dalton Trans.* **2006**, 3067−3076.
(31) Nar, H.; Messerschmidt, A.; Huber, R.; van de Kamp, M.; Canters, G. W. *J. Mol. Biol.* **1991**, *221*, 765−772.
(32) Walter, R. L.; Ealick, S. E.; Friedman, A. M.; Blake, R. C.; Proctor, P.; Shoham, M. *J. Mol. Biol.* **1996**, *263*, 730−751.
(33) van Gastel, M.; Coremans, J. W. A.; Sommerdijk, H.; van Hemert, M. C.; Groenen, E. J. J. *J. Am. Chem. Soc.* **2002**, *124*, 2035−2041.
(34) Vila, A. J.; Fernández, C. O. In *Handbook on Metalloproteins*; Bertini, I., Sigel, A., Sigel, H., Eds.; Marcel Dekker: New York, 2001; pp 813−856.
(35) Sinnecker, S.; Neese, F. *J. Comput. Chem.* **2006**, *27*, 1463−1475.
(36) Musiani, F.; Carloni, P.; Ciurli, S. *J. Phys. Chem. B* **2004**, *108*, 7495−7499.
(37) Li, H.; Webb, S. P.; Ivanic, J.; Jensen, J. H. *J. Am. Chem. Soc.* **2004**, *126*, 8010−8019.
(38) Libeu, C. A. P.; Kukimoto, M.; Nishiyama, M.; Horinouchi, S.; Adman, E. T. *Biochemistry* **1997**, *36*, 13160−13179.
(39) Dong, S. L.; Ybe, J. A.; Hecht, M. H.; Spiro, T. G. *Biochemistry* **1999**, *38*, 3379−3385.
(40) Carrell, C. J.; Sun, D. P.; Jiang, S. L.; Davidson, V. L.; Mathews, F. S. *Biochemistry* **2004**, *43*, 9372−9380.
(41) Yanagisawa, S.; Banfield, M. J.; Dennison, C. *Biochemistry* **2006**, *45*, 8812−8822.
(42) Hall, J. F.; Kanbi, L. D.; Harvey, I.; Murphy, L. M.; Hasnain, S. S. *Biochemistry* **1998**, *37*, 11451−11458.
(43) Hansen, D. F.; Gorelsky, S. I.; Sarangi, R.; Hodgson, K. O.; Hedman, B.; Christensen, H. E. M.; Solomon, E. I.; Led, J. J. *J. Biol. Inorg. Chem.* **2006**, *11*, 277−285.

Table 1. ^{1}H NMR Hyperfine Shifts of Cys−C$^\beta$**H**$_2$ in BCPs (Unit, ppm)

	δ_{hf}^{expt}	δ_{hf}^{calc1}	δ_{hf}^{calc2}	δ_{hf}^{calc3}	δ_{hf}^{calc4}	δ_{hf}^{calc5}	δ_{hf}^{calc6}	δ_{hf}^{calc7}	δ_{hf}^{calc8}
St H$^{\beta_1}$[a]	447.4	670.2	900.0	514.8	557.2	598.6	574.2	550.6	519.5
H$^{\beta_2}$[a]	372.6	654.2	505.4	595.8	620.3	578.9	532.7	405.6	377.3
H$_{av}$[b]	**410.0**	**662.7**	**702.7**	**555.3**	**579.8**	**588.8**	**553.5**	**478.1**	**448.4**
Pa H$^{\beta_1}$[a]	507.2	739.8	801.6	642.8	538.5	508.6	561.9	530.5	599.0
H$^{\beta_2}$[a]	386.9	690.3	475.3	644.7	601.2	588.5	527.6	506.7	580.9
H$_{av}$[b]	**447.1**	**715.1**	**638.5**	**643.8**	**569.9**	**548.6**	**544.8**	**518.6**	**590.0**
Pc H$^{\beta_1}$[a]	646.7	1106.1	887.3	1025.2	726.5	791.5	756.0	711.3	843.5
H$^{\beta_2}$[a]	486.1	790.2	554.3	707.5	652.3	575.6	530.5	506.7	612.3
H$_{av}$[b]	**566.4**	**948.1**	**720.8**	**866.4**	**689.4**	**683.6**	**643.3**	**609.0**	**727.9**
Az H$^{\beta_1}$[a]	846.5	887.1	993.1	872.8	835.1	801.4	798.4	740.2	761.6
H$^{\beta_2}$[a]	797.1	733.1	650.5	634.2	634.2	621.9	638.2	592.4	590.3
H$_{av}$[b]	**821.8**	**810.6**	**821.8**	**753.5**	**734.7**	**711.7**	**718.3**	**666.3**	**676.0**
Am H$^{\beta_1}$[a]				789.7				293.3	400.2
H$^{\beta_2}$[a]				679.1				277.5	369.5
H$_{av}$[b]				**734.4**				**285.4**	**384.9**
				theory vs experiment correlation (H$_{av}$)					
R		0.49	0.91	0.57	0.92	0.86	0.97	0.95	0.65
SD		134.1	39.1	135.4	37.9	47.9	24.6	34.0	113.3
P		>0.05	>0.05	>0.05	>0.05	>0.05	<0.05	=0.05	>0.05
				theory vs experiment correlation (H$^{\beta_1}$, H$^{\beta_2}$)[a]					
R		0.52	0.46	0.57	0.80	0.75	0.84	0.83	0.65
SD		138.4	191.8	146.3	61.6	75.3	62.7	67.4	116.1
P		>0.05	>0.05	>0.05	<0.05	<0.05	<0.01	=0.01	>0.05

[a] Experimental shift assignment based on computed shift. [b] H$_{av}$ is the average hyperfine shift for H$^{\beta_1}$, H$^{\beta_2}$. Note that only H$_{av}$ values are discussed in the text (independent of assignment). However, the correlations in this table are for both H$_{av}$ as well as for H$^{\beta_1}$, H$^{\beta_2}$ (taken to be the predicted shifts closest to experiment).

(up to C$^\beta$) and the NH atoms that are hydrogen bonded with the Cys ligand were also included in the geometry optimization as compared to the Calc7 model. The basis set scheme used in the geometry optimizations in the Calc2, Calc4, and Calc5 models was the same as that used for the NMR shift predictions, as described above. However, because of the larger size of the models used in the Calc6 and Calc7 (and Calc9 for Rc) investigations, the geometry optimization basis set was slightly smaller for the nonmetal heavy atoms: 6-311G* for the first coordination shell atoms and 6-31G* for the rest. For Am, only the Calc3, Calc7, and Calc8 models were used, since the reported experimental NMR hyperfine shift results (−13 to 43 ppm)[8] are for protons other than the Cys C$^\beta$H$_2$.

In addition to these QM shift calculations, we used Bader's AIM theory to help analyze some of the results. For convenience, we give here a very brief overview of this approach. According to AIM theory, each nucleus in a molecule is surrounded by a region called an atomic basin, which is bounded by a zero-flux surface in $\nabla\rho$, the gradient of the charge density, that defines an atomic boundary. When two atoms share some portion of their surfaces, a line of maximum electronic charge density is formed between the nuclei, and at the point where the shared surfaces intersect, the atomic interaction line, there is a saddle point in the charge density, $\rho(\mathbf{r})$, called a bond critical point. At this point, $\rho(\mathbf{r})$ is at a minimum along this atomic interaction line and at a maximum in the plane perpendicular to this line. In this manner, AIM theory identifies a unique line of communication between two chemically interacting nuclei and provides a unique point at which to probe or characterize the nature of the interaction. Every chemical bond has a bond critical point at which the first derivative of the charge density, $\rho(\mathbf{r})$, is zero.[13,14] The $\rho(\mathbf{r})$ topology is described by a real, symmetric, second-rank Hessian-of-$\rho(\mathbf{r})$ tensor, and the tensor trace is related to the bond interaction energy by a local expression of the virial theorem:

$$\mathrm{Tr(Hessian)} = \nabla^2\rho(\mathbf{r}) = [2\mathrm{G}(\mathbf{r}) + \mathrm{V}(\mathbf{r})](4m/\hbar^2) \qquad (5)$$

where $\nabla^2\rho(\mathbf{r})$ is the Laplacian of $\rho(\mathbf{r})$ and G($\mathbf{r}$) and V($\mathbf{r}$) are electronic kinetic and electronic potential energy densities, respectively. Negative and positive $\nabla^2\rho(\mathbf{r})$ values are associated with shared-electron (covalent) interactions and closed-shell (electrostatic) interactions, respectively. In the latter case, one can further evaluate the total energy density, H($\mathbf{r}$), at the bond critical point:

$$\mathrm{H}(\mathbf{r}) = \mathrm{G}(\mathbf{r}) + \mathrm{V}(\mathbf{r}) \qquad (6)$$

A negative H($\mathbf{r}$) is termed partial covalence, while a positive H($\mathbf{r}$) indicates a purely closed-shell, electrostatic interaction.[13,14,44] The bond critical point described above is also called a (3, −1) critical point, since it has three nonzero curvatures of $\rho(\mathbf{r})$, one of which is positive and two of which are negative. This type of critical point is associated with every chemical bond. In contrast, a ring critical point or (3, +1) critical point, having two positive and one negative curvatures, can be found in the inner area of a ring structure, and as discussed below, we find interesting correlations between these ring critical points and hyperfine shifts in the proteins of interest.[13,14] All critical point properties were calculated by using the AIM2000 program.[45]

Results and Discussion

Hyperfine Shift Calculations. We first investigated results for Az, Pc, Pa, St, and Am obtained by using the Calc1−Calc8 models, since these proteins have Cu ligands in the active site that are clearly hydrogen bonded. In the Calc1 models, there are only three strongly interacting equatorial ligands: two His and one Cys. A simplified model based on this motif previously enabled good predictions of the EPR g-tensor, as well as the hyperfine tensors of the His nitrogens in Az.[33] However, as shown in Table 1, the theory vs experiment correlation coefficient *R* for the large hyperfine shifts of the Cys C$^\beta$ protons (the average shifts for H$^{\beta 1}$ and H$^{\beta 2}$) observed in Az, Pc, Pa, and St is only about 0.5, using the X-ray structures, Calc1. *R* is improved upon a partial geometry optimization in which Cu and the Cys SCH$_2$ moiety are optimized, Calc2. However, in both cases, the statistical *p* values are >0.05, indicating no useful correlations from such calculations (even given the "most

(44) Arnold, W. D.; Oldfield, E. *J. Am. Chem. Soc.* **2000**, *122*, 12835−12841.
(45) Biegler-König, F. *AIM2000*, Version 2.0; University of Applied Science: Bielefeld, Germany, 2002.

Table 2. Geometric Parameters in Copper Centers of BCPs[a]

		X-ray	Calc4	Calc5	Calc6	Calc7
Az	$Cu-S^{Cys}$	2.13	2.17	2.15	2.16	2.16
	$Cu-S^{Met}$	2.95		3.05	3.02	2.99
	$Cu-N^{HisC}$	1.94		1.96	1.96	1.96
	$Cu-N^{HisN}$	1.96		2.00	2.00	1.99
	$Cu-O^{b}$	3.20		3.14	3.15	3.18
	$H^{\beta_1}-C-S-Cu$	72.1	70.9	70.5	70.4	71.6
	$H^{\beta_2}-C-S-Cu$	−48.1	−47.6	−48.3	−48.4	−47.3
Pc	$Cu-S^{Cys}$	2.07	2.13	2.13	2.13	2.14
	$Cu-S^{Met}$	2.82		2.83	2.87	2.88
	$Cu-N^{HisC}$	2.06		1.99	1.97	1.98
	$Cu-N^{HisN}$	1.91		1.97	1.98	1.97
	$Cu-O^{b}$	3.89		3.89	3.85	3.84
	$H^{\beta_1}-C-S-Cu$	69.8	64.2	67.2	68.2	67.8
	$H^{\beta_2}-C-S-Cu$	−50.3	−56.3	−53.2	−52.4	−52.9
Pa	$Cu-S^{Cys}$	2.13	2.17	2.15	2.15	2.15
	$Cu-S^{Met}$	2.71		2.71	2.77	2.78
	$Cu-N^{HisC}$	1.92		1.97	1.96	1.96
	$Cu-N^{HisN}$	1.95		1.98	1.98	1.98
	$Cu-O^{b}$	3.94		3.94	3.91	3.90
	$H^{\beta_1}-C-S-Cu$	72.0	68.3	68.2	69.7	68.9
	$H^{\beta_2}-C-S-Cu$	−48.0	−51.3	−51.7	−50.3	−51.0
St	$Cu-S^{Cys}$	2.18	2.18	2.17	2.17	2.17
	$Cu-O^{Gln}$	2.21		2.24	2.24	2.22
	$Cu-N^{HisC}$	2.04		2.02	1.98	1.97
	$Cu-N^{HisN}$	1.96		2.01	2.00	2.00
	$Cu-O^{b}$	3.97		3.97	3.99	4.02
	$H^{\beta_1}-C-S-Cu$	65.1	66.7	68.3	68.7	73.6
	$H^{\beta_2}-C-S-Cu$	−51.9	−52.5	−51.0	−50.8	−46.0

[a] The bond length is in Å; the H−C−S−Cu torsion angle is in degrees. [b] The carbonyl O is in the fifth coordination position.

favorable" H^{β_1,β_2} shift assignments). This suggests that the range of NMR hyperfine shifts observed experimentally may be influenced by the presence of additional groups that interact with the Cu(II) center. We thus next utilized larger models and six different sets of QM calculations. The key bond lengths and angles used in these models are listed in Table 2. The computed NMR shifts for the Cys C^{β} protons from all calculations (Calc1−Calc8) are shown in Table 1. The predicted hyperfine shifts of all experimentally observed protons are shown in Table 3, for the Calc3 (an X-ray structure model) and Calc7 (the largest geometry optimized model) investigations. The coordinates of all of the larger structures used in the calculations (Calc3−Calc7) are listed in Tables S2−25.

When the axial Met/Gln and the hydrogen-bonded Asn residues were included in the calculations (Calc3 models), a generally good theory vs experiment shift correlation was found, with $R^2 = 0.93$ and SD = 71.2 ppm or 8.0% of the whole 887.2 ppm range for all 53 experimentally observed shifts (and taking the H^{β_1}, H^{β_2} shift assignments to be those in closest accord with the calculations). When the average H^{β_1}, H^{β_2} values are used for the nonassigned protons, the statistics improve slightly to $R^2 = 0.94$ and SD = 51.8 ppm or 6.0% of the whole 862.5 ppm range for the 46 experimental shifts (Table 3). However, the slope is 1.20 (to be compared with an ideal value of 1.00) in both cases, and some δ_{hf} predictions for Cys−C^{β} hydrogen atoms have large errors (e.g., in Pc), as shown in Table 1. Because using eq 4 previously enabled accurate predictions of experimental shifts over a 6000 ppm range[7] with $R^2 = 0.99$ and slope = 1.05, the errors here may be (at least partly) associated with the uncertainties in the X-ray geometries of these proteins,[46] and indeed, in previous work, we found that ab initio calculations of NMR (and other spectroscopic) properties facilitated protein structure refinement.[22,47−50] We thus next began to use geometry optimization to see to what extent the shift predictions might be improved. Of course, as alluded to above, the specific assignments of H^{β_1} and H^{β_2} are not known experimentally, and individual Cys C^{β} proton shifts can have errors of ca. ±50−100 ppm as a result of the extremely broad (up to ∼1.2 MHz) line widths seen in the experimental solution NMR spectra.[9−11] So, we use here the average shift of H^{β_1}, H^{β_2} to assess the accuracy of a given calculation, since this value is obviously independent of the specific assignment.

By optimizing just the Cys−SCH_2 moiety (Calc4 model), we find a large improvement for the average Cys−SC**H**$_2$ δ_{hf} predictions, with the SD (in Az, Pc, Pa, and St) dropping from 135.4 to 37.9 ppm (Table 1). The biggest improvement (∼200 ppm) is with Pc, where as can be seen in Table 2, the $Cu-S^{Cys}$ bond length undergoes the largest (0.06 Å) change. A comparison of all of the experimental shifts with the results of the Calc4 model predictions shows that the slope improves from 1.20 (Calc3) to 1.11 (Calc4); R^2 improves marginally, from 0.94 (Calc3) to 0.95 (Calc4), and the SD decreases, from 51.8 (Calc3) to 41.9 ppm (Calc4). Each successive model (Calc5−Calc7) included more structural units or extended the size of the geometry optimization (Table S1). As shown in Table 2, the calculated bond lengths for all three strong coordination bonds: $Cu-S^{Cys}$, $Cu-N^{HisN}$ (the N-terminal His ligand), and $Cu-N^{HisC}$ (the C-terminal His ligand), all basically converge to within 0.01 Å of each other at Calc5, as shown, for example, in Figure 1, for $Cu-S^{Cys}$. Convergence for the bond length of the weak $Cu-S^{Met}$ bond is ca. 0.05 Å, the same as the Cu−O distance (the carbonyl O in the peptide bond located in the fifth coordination position, trans to the axial Met/Gln ligand). The dihedral angles (H−C−S−Cu) also generally converge to within ∼1° at Calc5, as again shown in Table 2.

Further improvements in average shift predictions were obtained with the larger, optimized Calc6 and Calc7 models, with the Calc7 model correctly reproducing the order of the experimental average hyperfine shifts of the Cys C^{β} protons (Table 1). This clearly indicates the importance of bonding effects from the residue in the fifth ligand position (included in Calc6 and Calc7), together with the effects of other residues H-bonded to the first coordination shell, including those hydrogen-bonded to His ligands. The Calc7 predictions for all 46 experimental shifts (using only the average shifts for the nonstereospecifically assigned protons) are now very good: $R^2 = 0.96$, slope = 0.98 (to be compared with the ideal value of 1.00), and a SD = 31.4 ppm, or 3.6% of the whole 862.5 ppm shift range seen experimentally. Comparisons with the results from Calc8 models, which have the same size as the Calc7 models, but without geometry optimization (Table 1), clearly indicate that geometry optimization is still important for good predictions of NMR hyperfine shifts in BCPs, even when very large structural units are used in the calculations, since the R^2 value degrades to 0.65 for Calc8. This is consistent with the

(46) http://www.rcsb.org/pdb/static.do?p=general_information/about_pdb/nature_of_3d_structural_data.html.

(47) McMahon, M. T.; deDios, A. C.; Godbout, N.; Salzmann, R.; Laws, D. D.; Le, H. B.; Havlin, R. H.; Oldfield, E. *J. Am. Chem. Soc.* **1998**, *120*, 4784−4797.
(48) Zhang, Y.; Oldfield, E. *J. Am. Chem. Soc.* **2004**, *126*, 4470−4471.
(49) Zhang, Y.; Oldfield, E. *J. Am. Chem. Soc.* **2004**, *126*, 9494−9495.
(50) Mao, J. H.; Mukherjee, S.; Zhang, Y.; Cao, R.; Sanders, J. M.; Song, Y. C.; Zhang, Y. H.; Meints, G. A.; Gao, Y. G.; Mukkamala, D.; Hudock, M. P.; Oldfield, E. *J. Am. Chem. Soc.* **2006**, *128*, 14485−14497.

Table 3. Solution ^{1}H NMR Chemical Shifts in BCPs (Unit, ppm)

	St			Pa			Pc			Az			Am			Rc[b]	
a	δ_{hf}^{expt}	δ_{hf}^{calc3}	δ_{hf}^{calc7}	δ_{hf}^{expt}	δ_{hf}^{calc3}	δ_{hf}^{calc7}	δ_{hf}^{expt}	δ_{hf}^{calc3}	δ_{hf}^{calc7}	δ_{hf}^{expt}	δ_{hf}^{calc3}	δ_{hf}^{calc7}	δ_{hf}^{expt}	δ_{hf}^{calc3}	δ_{hf}^{calc7}	δ_{hf}^{expt}	δ_{hf}^{calc9}
Cys H^{α}	−12.6	14.7	−4.1		−5.1	−2.2	−13.4	−11.8	−2.2	−12.8	−10.3	−9.3	9.6	6.1	−0.4		−10.9
H^{β_1}	372.6	514.8	405.6	507.2	644.7	530.5	646.7	1025.2	711.3	846.5	872.8	761.6		789.7	293.3	293.7	625.1
H^{β_2}	447.4	595.8	550.6	386.9	642.8	506.7	486.1	707.5	506.7	797.1	634.2	590.3		679.1	277.5	236.8	304.2
HisN H^{α}		−1.3	−1.3		3.5	1.6	13.2	1.6	0.6		10.1	10.1		−0.4	−0.4		1.6
H^{β_1}		−11.7	−10.7		−8.0	−8.9	−4.3	−8.9	−8.9		−4.2	−7.3	−12.7	−7.9	−4.1		−8.0
H^{β_2}		−2.3	1.5		−2.2	−0.3		−0.3	2.5		−4.2	−3.2	−4.9	−0.4	−0.4		16.9
H^{ϵ_1}	22.4	19.4	22.2	24.5	26.3	23.4	28.4	18.7	22.5	27.2	17.2	13.1		21.0	5.2	29.6	7.3
H^{ϵ_2}	15.9	10.9	13.8	12.5	10.1	12.0	19.7	9.2	9.2	15.4	8.0	9.0	14.1	2.4	5.2		
H^{δ_2}	40.9	20.4	26.0	39.3	21.5	22.5	39.5	12.0	16.8	43.2	19.2	21.3	35.6	7.0	−4.1	42.3	20.7
HisC H^{ϵ_1}	33.6	23.2	28.8	24.8	21.5	25.3	27.9	14.9	21.5	39.9	34.5	35.6		20.0	14.5	23.3	23.6
H^{ϵ_2}		26.0	26.9		24.4	24.4		8.2	13.9	15.3	18.2	18.2		17.2	9.8	10.8	8.3
H^{δ_2}	48.0	25.1	27.9	46.5	29.1	32.0	44.6	12.0	15.8	47.1	21.3	22.3	42.6	13.5	8.0	51.4	19.8
Met H^{γ_1}					7.3	−2.2	21.8	−3.2	−3.2		−2.2	−2.2	9.3	4.2	−0.4		−2.2
H^{γ_2}					19.6	−2.2	10.8	−2.2	−5.1		−4.2	−5.2	8.6	−3.2	−3.2		−6.1
H^{ϵ}				11.3	−4.2	−4.2		−4.2	−4.2		−3.2	−3.2		−3.2	−3.2	7.3	−3.2
Asn H^{N}	−25.5	−57.8	−64.4	−24.6	−45.1	−58.4	−29.2	−60.3	−56.5	−40.7	−39.9	−42.0		−40.4	−34.8	−30.6	−31.9
H^{α}	12.4	23.2	20.3	12.5	17.7	20.6	12.8	17.7	13.9	15.2	15.2	15.2		15.4	7.0	14.5	7.3

[a] Tentative assignments of H^{β_1}/H^{β_2} and $H^{\gamma_1}/H^{\gamma_2}$ are made to let them have the same order as reported in experiment. [b] The Asn residue in other BCPs corresponds to Ser in Rc. The experimental HisN H^{ϵ_2} shift was reassigned to HisC H^{ϵ_2} shift due to a tentative structure with the imidazolate HisN.

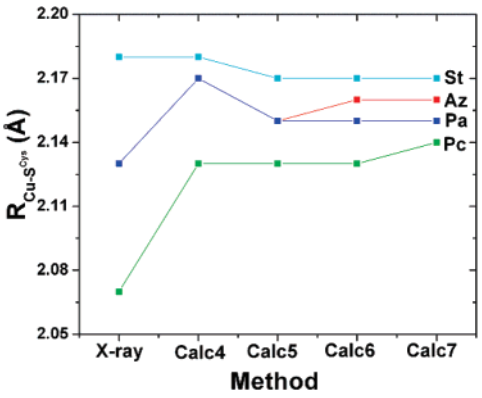

Figure 1. Cu−S^{Cys} bond lengths from experiment and calculations in Az (red), Pa (blue), Pc (green), and St (cyan).

results of previous investigations,[22,47−50] showing that QM refinement of protein X-ray structures is generally needed to provide the best property predictions, at least in the case of metal-binding sites.

We also investigated other factors, which might be expected to have an effect on the NMR hyperfine shift predictions. For Pa and St, the X-ray structures were of the same species as used in the NMR experiments, but for Am, Az, and Pc, the X-ray/NMR results were on proteins from different species. This was because the X-ray structures from the same species as used in the NMR experiments were of lower resolution than those used here. For example, the 4AZU[31] structure of Az from *Pseudomonas aeruginosa* has a resolution of 1.90 Å, 0.3 Å lower than the 1.60 Å resolution of the 1NWP (*Pseudomonas putida*) structure used in our calculations. However, even though the proteins are from different species, the sequences of the residues included in the Calc7 models (for Am and Pc) are the same as those that are present in the proteins used for the NMR experiments. We also investigated another recently published Az structure, 2CCW,[30] that has even higher resolution (1.13 Å) but again is from another species (*Achromobacter xylosoxidans*). For comparison, we used the same Calc7 models with these three different starting structures (4AZU, 1NWP, and 2CCW) for Az. As shown in Table S26, the calculated NMR hyperfine shifts from using 4AZU have an inferior correlation ($R^2 = 0.91$) with the experimental NMR results than do those obtained by using 1NWP ($R^2 = 0.99$). The Calc7 results from using even higher resolution structure 2CCW are essentially the same as from using 1NWP. In addition, the Calc7-optimized geometry for Am here is also close to that of a higher resolution structure (2OV0)[29] deposited very recently (Table S27). These results further support the use of current Calc7 models.

Although the key factor in choosing the Calc7 models was based on the predictions of the large Cys C^{β} proton NMR hyperfine shifts, the methods also offer a good explanation for the relatively smaller shifts seen with other protons. For instance, as shown in Table 3, for the conserved Asn residue in Az, Pc, Pa, St, and Am, the amide proton and the Cα proton were consistently predicted to have negative and positive hyperfine shifts, respectively, as observed experimentally.[8−11] The Cys C^{α} protons in these proteins were predicted to have a negative hyperfine shift, due to their proximity to the large positive spin densities of the Cys C^{β} protons.[10] Hyperfine shift predictions for His protons are generally good, except for the $C^{\delta 2}$ protons, where the hyperfine shift range is small, as it is with many other residues, and in some cases, assignments are uncertain.[8,10,11,51] The large Cys C^{β} proton shift range should thus be a more reliable structural probe. In fact, as shown in Table 3, the Cys C^{β} proton NMR hyperfine shifts have large differences between the small Calc3 and large Calc7 models, while the other proton shifts between these two models are generally not very different.

The above results indicate that all of the active site residues included in the calculations have some effects on the NMR hyperfine shifts predictions, with the axial ligands, residues hydrogen-bonded to Cys, and the carbonyl oxygen located in the fifth coordination position[35−43,52,53] being of particular importance. However, the results shown here also indicate that residues hydrogen-bonded to His are important and need to be taken into account to reproduce the experimental shifts. As shown in Table 1, for Am, there is a large difference (349.5 ppm) between the calculated average Cys C^{β} proton NMR

(51) Sato, K.; Dennison, C. *Biochemistry* **2002**, *41*, 120−130.
(52) Garner, D. K.; Vaughan, M. D.; Hwang, H. J.; Savelieff, M. G.; Berry, S. M.; Honek, J. F.; Lu, Y. *J. Am. Chem. Soc.* **2006**, *128*, 15608−15617.
(53) George, S. D.; Basumallick, L.; Szilagyi, R. K.; Randall, D. W.; Hill, M. G.; Nersissian, A. M.; Valentine, J. S.; Hedman, B.; Hodgson, K. O.; Solomon, E. I. *J. Am. Chem. Soc.* **2003**, *125*, 11314−11328.

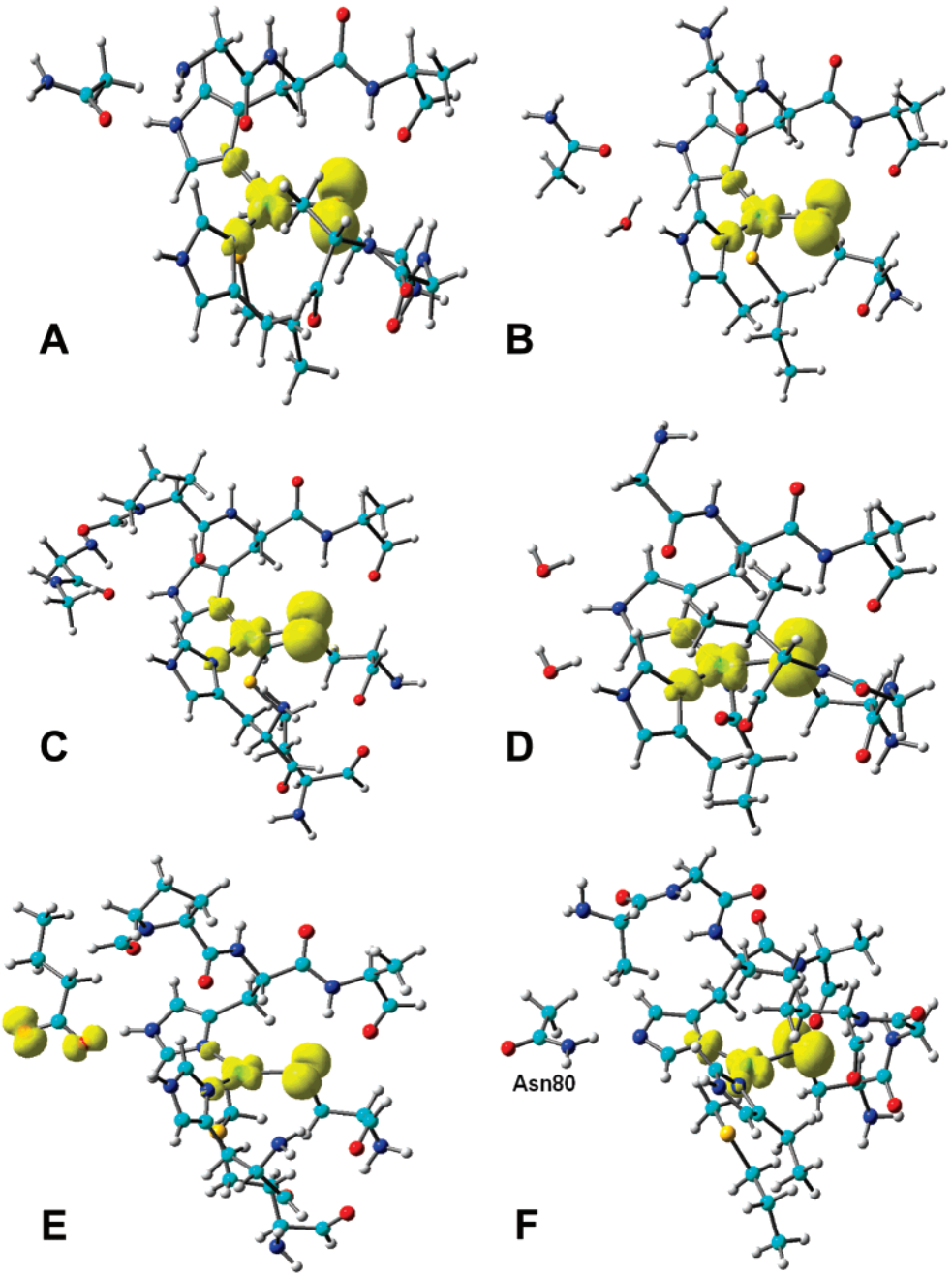

Figure 2. (A) Spin densities from Calc7 model calculations (contour value = ±0.004 au) for (A) Az, (B) Pa, (C) Pc, (D) St, (E) Am, and (F) Rc (Calc9 model). Atom color scheme: Cu, green; C, cyan; N, blue; O, red; S, yellow; and H, gray.

hyperfine shifts ($^{av}\delta_{hf}^{calc}$) from the smaller (Calc3) model and the larger (Calc8) model, even when using the same basic geometry. This difference is much larger than the differences (53.8−138.5 ppm) seen with Az, Pc, Pa, and St. One likely origin of the major difference between the Am and other BCP results appears to originate in the nature of the hydrogen bond partner to the N-terminal His ligand. It is a negatively charged Glu residue in Am, but in Az, Pc, Pa, and St, it is a neutral residue or a water molecule. A calculation of a modified Calc8 model for Am that only removed this Glu, but kept all other residues, yielded an $^{av}\delta_{hf}^{calc}$ value of 687.4 ppm. Clearly, then, this Glu residue is a major contributor to the large difference between the $^{av}\delta_{hf}^{calc}$ of 384.9 (with Glu) and 687.4 ppm (without Glu) and accounts for 87% of the total difference between the Calc3 and the Calc8 models. This effect is reflected in the spin density distributions. As shown in Figure 2A−D, the general features of the spin density distribution in other BCPs (Az, Pa, Pc, and St) are the same, as found with smaller models,[54,55] and consist primarily of densities in a Cu d_{x2-y2} orbital, a Cys sulfur p orbital, as well as some His nitrogen orbitals. However, in Am, there are also large spin densities in the H-bonded Glu residue (Figure 2E). In addition, for Pa and Pc, the only difference between Calc6 and Calc7 models is the inclusion of the N−His hydrogen-bonding partners in the Calc7 models, which again results in significant improvement in the NMR hyperfine shift predictions (Table 1), due to incorporation of the His hydrogen-bonded partners.

(54) Sugimori, K.; Shuku, T.; Sugiyama, A.; Nagao, H.; Sakurai, T.; Nishikawa, K. *Polyhedron* **2005**, *24*, 2671−2675.
(55) Solomon, E. I. *Inorg. Chem.* **2006**, *45*, 8012−8025.

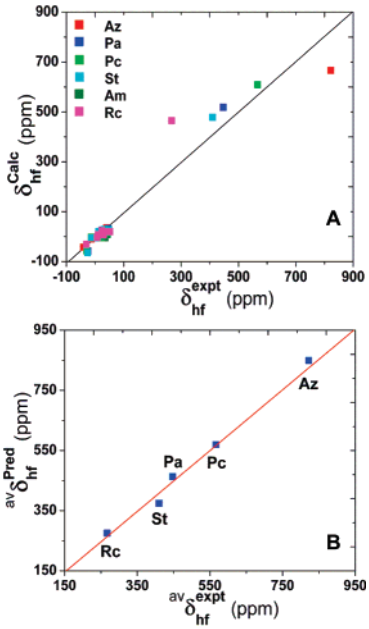

Figure 3. (A) QM calculated vs experimental NMR hyperfine shifts in BCPs. (B) Predicted NMR hyperfine shifts using eq 8 vs experimental data in BCPs.

As compared with the BCPs discussed above, Rc has several unusual features, including the highest redox potential (680 mV) among BCPs,[32] and the smallest Cys C^{β} proton NMR hyperfine shifts[11] (Table 3). All eight X-ray structures (PDB #: 1RCY, 2CAK, 1A8Z, 1A3Z, 2CAL, 1E30, 1GY2, and 1GY1) for wild-type or mutated Rc show that Asn80 is hydrogen-bonded to the N-terminal His (His85), but there are two possible bonding modes. This is different to the situations found with other BCPs, where there are unambiguous H-bond patterns. In two structures (1RCY and 1A3Z), the Asn80 side chain's C═O group forms an H-bond with His85, but in six other structures (including the highest resolution structure 2CAK), the Asn80 side chain is flipped, and thus, it is the Asn80 side chain's NH_2 group forming the H-bond with His85, as shown in Figure 2F, a mode not seen in other BCPs. These structures suggested the possibility that this interaction might be sufficiently strong to generate an imidazolate ligand (Im^-), similar to the Cu(II)−Im^- motif seen with oxidized CuZnSOD (SOD, superoxide dismutase).[56] Certainly, the very high redox potential as well as the very small hyperfine shifts indicate a very unusual interaction. We thus first investigated the 1RCY structure model for Rc, finding as shown in Table 4, a predicted average Cys C^{β} proton hyperfine shift from a Calc3 model of 746.3 ppm, about a 500 ppm deviation from the experimental value of 267.1 ppm. Even with the Calc7 model, which has all hydrogen-bonded partners with all of the Cu ligands, the error was still large (440 ppm), much larger than those found with other BCPs using the same Calc7 models: 42.6 ppm for Pc, 68.1 ppm for St, 71.5 ppm for Pa, and 155.5 ppm for Az. Inclusion of Asn80 and Im^- with the 2CAK geometry yielded, however, a significant improvement (509.7 ppm) as compared with the Calc7 prediction using 1RCY (with Im^0, 707.5 ppm), and when this whole Im^- ligand (up to C^{β}) and the NH atoms that are hydrogen-bonded with the Cys ligand were also included in the geometry optimization in this unusual case (Calc9 model), the result improved further, to 464.7 ppm (Table 4). This supports a tentative assignment of a very strongly hydrogen-bonded (Asn80) $NH_2\cdots N^{\epsilon}$ (His85), in which the interaction between the Cu center and the His ligand is strengthened, resulting in a longer Cu−S^{Cys} bond (Table 5) and a small hyperfine shift. This effect of a negatively charged Im^- (of the N-terminal His ligand) on structure and hyperfine shift is similar to that of a negatively charged Glu (H-bonded to again, an N-terminal His ligand) in Am, where a longer Cu−S^{Cys} bond and a smaller hyperfine shift were also found (Table 5). The coordinates of all Rc structures used in the calculations are listed in Tables S28−S36. As shown in Figure 3A, with these geometry-optimized large models of Az, Pc, Pa, St, Am, and Rc, the predictions of all 53 experimental shifts (using only the average shifts for the nonstereospecifically assigned protons) have a very good correlation with experiment, $R^2 = 0.94$, slope = 1.01 (to be compared with the ideal value of 1.00), and a SD = 40.5 ppm or 4.7% of the whole 862.5 ppm shift range seen experimentally. These results also fit the same correlation line (Figure S1) seen previously with heme proteins and model systems,[7] indicating the good overall accuracy of the methods employed.

On the basis of the largest models investigated here, the large differences in geometries seen in the X-ray structures of different BCPs in their oxidized forms are significantly decreased in the geometry optimized structures. This suggested that it might be possible to use these optimized geometric properties to predict shifts, using the empirical approach described previously.[11] The properties of interest are the displacement of Cu from the N^{His}-CuN^{His} plane (ΔCu),[57] the angle between the $N^{His}CuN^{His}$ and $S^{Cys}CuS^{Met}(O^{Gln})$ planes (ϕ),[58,59] and the angle formed by the $N^{His}CuN^{His}$ plane and Cu−S^{Cys} vector (α). As observed previously,[11] the average experimental Cys C^{β} proton hyperfine shift is not correlated with $R_{Cu-S}{}^{Cys}$, ΔCu, ϕ, or α alone. However, the following relationship using a combination of $R_{Cu-S}{}^{Cys}$ and

Table 4. ^{1}H NMR Hyperfine Shifts of Cys−$C^{\beta}\mathbf{H}_2$ in Rc (Unit, ppm)

	$\delta_{hf}{}^{expt}$	$\delta_{hf}{}^{calc3}$	$\delta_{hf}{}^{calc4}$	$\delta_{hf}{}^{calc5}$	$\delta_{hf}{}^{calc6}$	$\delta_{hf}{}^{calc7}$	$\delta_{hf}{}^{calc8}$	$\delta_{hf}{}^{calc9}$
				1RCY				
$H^{\beta_1}{}^a$	297.3	778.3	760.5	777.7	788.2	740.0	706.5	
$H^{\beta_2}{}^a$	236.8	714.2	749.9	679.1	667.6	674.9	634.7	
$H_{av}{}^b$	**267.1**	**746.3**	**755.2**	**728.4**	**727.9**	**707.5**	**670.6**	
				2CAK				
$H^{\beta_1}{}^a$	297.3	869.3	951.7			660.5	565.7	625.1
$H^{\beta_2}{}^a$	236.8	677.8	607.9			358.8	414.4	304.2
$H_{av}{}^b$	**267.1**	**773.6**	**779.8**			**509.7**	**490.1**	**464.7**

[a] Experimental shift assignment based on computed shift. [b] H_{av} is the average hyperfine shift for H^{β_1}, H^{β_2}. Note that only H_{av} values are discussed in the text (independent of assignment).

Table 5. NMR Hyperfine Shifts and Structural Parameters[a]

protein	$^{av}\delta_{hf}{}^{expt}$ (ppm)	$R_{Cu-S}{}^{Cys}$ (Å)	ΔCu (Å)	ϕ (°)	α (°)	$^{av}\delta_{hf}{}^{pred}$ (ppm)
Az	821.8	2.16	0.19	79.6	13.9	849.7
Pc	566.4	2.14	0.33	79.1	24.0	569.4
Pa	447.1	2.15	0.33	76.5	23.7	463.4
St	410.0	2.17	0.30	83.1	21.4	374.6
Am		2.19	0.25	80.5	17.7	331.2
Rc	267.1	2.19	0.30	80.3	21.7	275.2

[a] Results are from Calc7 models for Az, Pc, Pa, St, Am, and Calc9 models for Rc. ΔCu is the displacement of Cu from the $N^{His}CuN^{His}$ plane. ϕ is the angle between $N^{His}CuN^{His}$ and $S^{Cys}CuS^{Met}(O^{Gln})$ planes. α is the angle formed by the $N^{His}CuN^{His}$ and Cu−S^{Cys} vector. $^{av}\delta_{hf}{}^{pred}$ data are calculated using eq 8.

(56) Holm, R. H.; Kennepohl, P.; Solomon, E. I. *Chem. Rev.* **1996**, *96*, 2239−2314.

Table 6. Bond Critical Point Properties in BCPs[a]

protein	bond	*R* (Å)	$\rho(\mathbf{r})$ (au)	G(**r**) (au)	V(**r**) (au)	$\nabla^2\rho(\mathbf{r})$ (au)	H(**r**) (au)
Az	$Cu-S^{Cys}$	2.16	0.09404	0.09779	−0.12092	0.2986	−0.02313
	$Cu-N^{HisN}$	1.96	0.08727	0.11972	−0.13144	0.4320	−0.01172
	$Cu-N^{HisC}$	1.99	0.09314	0.12983	−0.14382	0.4634	−0.01399
	$Cu-S^{Met}$	2.99	0.01932	0.01284	−0.01572	0.03983	−0.00288
Pc	$Cu-S^{Cys}$	2.14	0.09784	0.10411	−0.12901	0.3169	−0.02490
	$Cu-N^{HisN}$	1.98	0.09121	0.12798	−0.14116	0.4592	−0.01318
	$Cu-N^{HisC}$	1.97	0.08796	0.12200	−0.13364	0.4414	−0.01164
	$Cu-S^{Met}$	2.88	0.02478	0.01641	−0.02140	0.04569	−0.00499
Pa	$Cu-S^{Cys}$	2.15	0.09523	0.09847	−0.12225	0.2987	−0.02378
	$Cu-N^{HisN}$	1.96	0.08918	0.12421	−0.13648	0.4477	−0.01227
	$Cu-N^{HisC}$	1.98	0.09334	0.12872	−0.14274	0.4588	−0.01402
	$Cu-S^{Met}$	2.78	0.02926	0.02016	−0.02657	0.05500	−0.00641
St	$Cu-S^{Cys}$	2.17	0.09152	0.09399	−0.11611	0.2875	−0.02212
	$Cu-N^{HisN}$	1.97	0.08483	0.11662	−0.12703	0.4248	−0.01041
	$Cu-N^{HisC}$	2.00	0.09249	0.12632	−0.14008	0.4502	−0.01376
	$Cu-O^{Gln}$	2.22	0.04492	0.05401	−0.05544	0.2103	−0.00143
Am	$Cu-S^{Cys}$	2.19	0.08850	0.08876	−0.10863	0.2664	−0.01987
	$Cu-N^{HisN}$	1.98	0.08757	0.12193	−0.13353	0.4413	−0.01160
	$Cu-N^{HisC}$	2.01	0.08110	0.11127	−0.12041	0.4085	−0.00914
	$Cu-S^{Met}$	3.02	0.01815	0.01219	−0.01472	0.03868	−0.00253
Rc	$Cu-S^{Cys}$	2.19	0.08751	0.08763	−0.10800	0.2690	−0.02037
	$Cu-N^{HisN}$	1.96	0.09601	0.12551	−0.14149	0.4381	−0.01598
	$Cu-N^{HisC}$	2.05	0.07584	0.09829	−0.10593	0.3626	−0.00764
	$Cu-S^{Met}$	2.88	0.02387	0.01586	−0.02048	0.04493	−0.00462

[a] From Calc7 results for Az, Pc, Pa, St, Am, and Calc9 results for Rc.

α was recently found to give good predictions of the $^{av}\delta_{hf}^{expt}$ data:[11]

$$1/^{av}\delta_{hf}{}^{expt} = a\, R_{Cu-S}{}^{Cys} + b\, \mathrm{tg}\,\alpha + c \qquad (7)$$

where *a*, *b*, and *c* are fitting parameters. Using the data from the large geometry-optimized models (Table 5), we find that this relationship gives good predictions: $R^2 = 0.82$ (for Az, Pc, Pa, and St) and 0.99 (for Az, Pc, Pa, St, and Rc). However, the projection of the major spin densities in the Cu d_{x2-y2} orbital (Figure 2) onto the $Cu-S^{Cys}$ vector (the major source of the spin densities of Cys C^{β} protons) may be better described by a cos α term than the tg α term in eq 7. Indeed, including a cos α term:

$$1/^{av}\delta_{hf}{}^{expt} = a\, R_{Cu-S}{}^{Cys} + b\, \cos\alpha + c \qquad (8)$$

gives even better fittings: $R^2 = 0.99$ (for Az, Pc, Pa, and St) and 0.99 (for Az, Pc, Pa, St, and Rc). The fitting parameters were $a = 0.0457$ Å^{-1} ppm^{-1}, $b = 0.02612$ ppm^{-1}, and $c = 0.07218$ ppm^{-1}, and the predicted hyperfine shifts ($^{av}\delta_{hf}^{pred}$) have a SD of 24.3 ppm or only 4.4% for an experimental range of 554.7 ppm, as shown in Figure 3B. Using eq 8, the $^{av}\delta_{hf}^{pred}$ for Am is 331.2 ppm, very close to the Calc7 prediction, 285.4 ppm (Table 1).

AIM Theory Results. To investigate the structural effects on NMR hyperfine shifts in more depth, we next employed AIM theory[13,14] to see if electronic effects from weakly interacting groups might correlate with the hyperfine shifts. For each of the four Cu coordination bonds, a bond critical point was identified and the calculated bond critical point properties are listed in Table 6. The Laplacian results for the three strong equatorial coordination bonds ($Cu-S^{Cys}$, $Cu-N^{HisN}$, and $Cu-N^{HisC}$) as well as the axial $Cu-S^{Met}$ (in Az, Pc, Pa, Am, Rc)/ $Cu-O^{Gln}$ (in St) bonds were all positive, indicating that (in AIM terminology) they are of an electrostatic nature. However, all of the total energy densities, H(**r**), were negative, suggesting "partial covalence".[44] Nevertheless, the bond critical point properties of the axial bonds were smaller than those of the three equatorial coordination bonds, consistent with the fact that the axial coordination bonds are relatively weak. It is interesting to note that for Az, Pc, Pa, and St, which have neutral His ligands and H-bonded residues, the sum of the charge densities $\rho(\mathbf{r})$ at the bond critical points in the three equatorial and one axial coordination bonds has an excellent correlation with both the experimental and the computed average NMR hyperfine shifts (of the Cys C^{β} protons), with $R^2 = 0.97$ and 0.95, respectively, using an exponential decay fit. Its relation with the experimental shifts is illustrated in Figure 4A. In addition, the sums of G(**r**) and V(**r**) in these four bonds correlate with $^{av}\delta_{hf}^{expt}$ in the same manner, having $R^2 = 0.88$ and 0.92, respectively. However, if only the three strong equatorial coordination bonds are considered, $\Sigma\rho(\mathbf{r})$ is not correlated with $^{av}\delta_{hf}$. This provides further evidence that weak ligands play an important role in affecting the overall spin density (or hyperfine shift) variations in the different proteins, as suggested in Figure S2. We also found excellent correlations between $^{av}\delta_{hf}^{expt}$ and

Table 7. Ring Critical Point Properties in Cu···H Interactions in BCPs[a]

protein	$\rho(\mathbf{r})$ (au)	G(**r**) (au)	V(**r**) (au)	$\nabla^2\rho(\mathbf{r})$ (au)	H(**r**) (au)	$d_{Cu\cdots X}$ (Å)	$d_{X\cdots H}$ (Å)
Az	0.00293	0.00168	−0.00119	0.00870	0.00049	2.92	1.42
Pc	0.00322	0.00238	−0.00166	0.01237	0.00072	2.88	1.36
Pa	0.00559	0.00410	−0.00301	0.02070	0.00109	2.88	1.38
St	0.00781	0.00641	−0.00520	0.03047	0.00121	2.08	1.40
Am	0.00335	0.00195	−0.00139	0.01007	0.00056	3.03	1.66
Rc	0.00563	0.00359	−0.00266	0.01812	0.00093	2.27	1.60

[a] Results are from Calc7 models for Az, Pc, Pa, St, Am, and Calc9 models for Rc. X is the ring critical point.

(57) Lu, Y.; LaCroix, L. B.; Lowery, M. D.; Solomon, E. I.; Bender, C. J.; Peisach, J.; Roe, J. A.; Gralla, E. B.; Valentine, J. S. *J. Am. Chem. Soc.* **1993**, *115*, 5907−5918.
(58) LaCroix, L. B.; Randall, D. W.; Nersissian, A. M.; Hoitink, C. W. G.; Canters, G. W.; Valentine, J. S.; Solomon, E. I. *J. Am. Chem. Soc.* **1998**, *120*, 9621−9631.
(59) Pierloot, K.; De Kerpel, J. O. A.; Ryde, U.; Olsson, M. H. M.; Roos, B. O. *J. Am. Chem. Soc.* **1998**, *120*, 13156−13166.

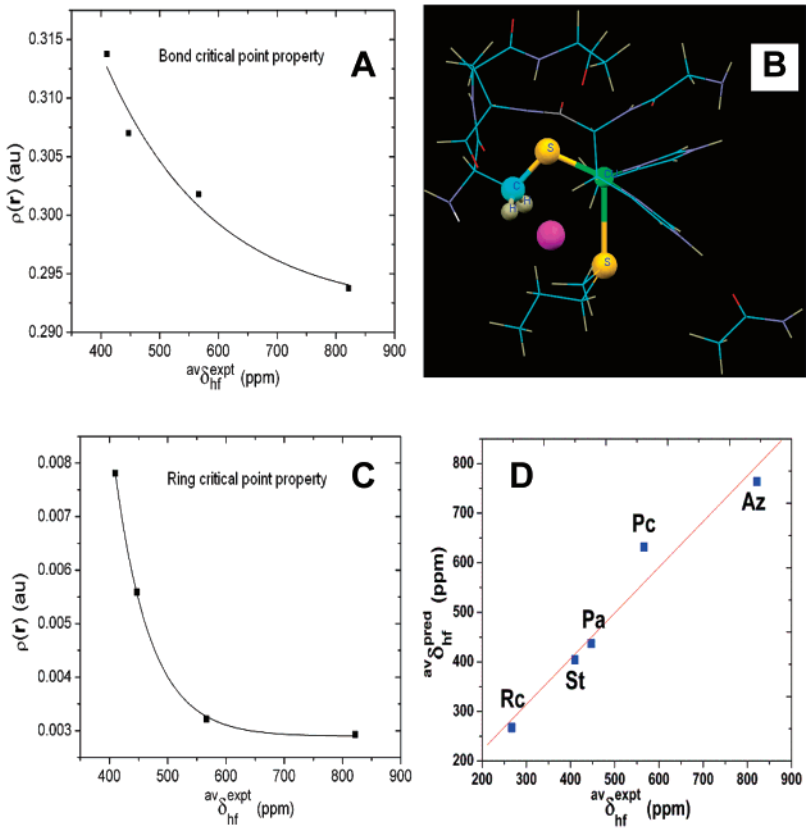

Figure 4. (A) Plot of the sum of $\rho(\mathbf{r})$ at bond critical points of the four typical coordination bonds vs $^{av}\delta_{hf}^{expt}$ of the Cys C$^{\beta}$ protons for Az, Pc, Pa, and St. (B) A ring critical point (purple sphere) in Az. (C) Plot of $\rho(\mathbf{r})$ at the ring critical points involving Cu···H(−C$^{\beta}$, Cys) vs $^{av}\delta_{hf}^{expt}$ of the Cys C$^{\beta}$ protons for Az, Pc, Pa, and St. (D) Plot of $^{av}\delta_{hf}^{pred}$ calculated with eq 9 using G($\mathbf{r}$) of bond critical points and ring critical point vs $^{av}\delta_{hf}^{expt}$.

the $\rho(\mathbf{r})$, G($\mathbf{r}$), V($\mathbf{r}$), and $\nabla^2\rho(\mathbf{r})$ properties at the axial bond critical points (R^2 = 0.96, 0.98, 0.98, and 0.98, respectively). However, results for Am and Rc (which have either a negatively charged His or a negatively charged H-bond partner) do not follow these correlations, indicating a more significant role of these charged groups on the electronic properties than that of axial ligands, as also observed with the NMR hyperfine shift properties discussed above. In addition to the bond critical point results, we also detected a ring critical point in the region surrounded by Cu, the Cys SCH_2, and S^{Met}/O^{Gln} in each system, as illustrated in Figure 4B for Az. The AIM properties at the ring critical points are very well-correlated with the (average) experimental NMR hyperfine shifts of the Cys C$^{\beta}$ protons, $^{av}\delta_{hf}^{expt}$. For charge densities (Figure 4C), the correlation coefficient (for an exponential decay fit) is R^2 = 0.9998, and the correlation coefficients for G($\mathbf{r}$), V($\mathbf{r}$), $\nabla^2\rho(\mathbf{r})$, and H($\mathbf{r}$) are all in the range 0.992−0.997. Again, these correlations are for BCPs with neutral His ligands and H-bonded residues (Az, Pc, Pa, and St), consistent with the results seen with the bond critical point properties. However, when bond critical point (bcp) properties and ring critical point (rcp) properties were used together, the $^{av}\delta_{hf}^{expt}$ results for all BCPs can be predicted using the following equation:

$$\ln {}^{av}\delta_{hf}{}^{expt} = a \ln\sum(\text{bcp}) + b \ln(\text{rcp}) + c \qquad (9)$$

with R^2 = 0.93, 0.97, and 0.94 for $\rho(\mathbf{r})$, G($\mathbf{r}$), and |V($\mathbf{r}$)|, respectively. The fitting parameters are listed in Table S37, and the predicted average Cys C$^{\beta}$ proton NMR hyperfine shifts from eq 9, using bcp and rcp data for $\rho(\mathbf{r})$, G($\mathbf{r}$), and |V($\mathbf{r}$)|, are shown in Table 8. This correlation is illustrated by the results for G($\mathbf{r}$) shown in Figure 4D, indicating that excellent theory−experiment correlations can be made, based on the critical point properties.

Table 8. Predictions of Cys C$^{\beta}$ Proton Hyperfine Shifts Using AIM Properties[a]

protein	$^{av}\delta_{hf}^{expt}$ (ppm)	$^{av}\delta_{hf}^{pred1}$ (ppm)	$^{av}\delta_{hf}^{pred2}$ (ppm)	$^{av}\delta_{hf}^{pred3}$ (ppm)
Az	821.8	763.7	723.1	710.4
Pc	566.4	631.5	649.9	660.2
Pa	447.1	437.3	470.6	459.7
St	410.0	404.4	383.7	398.5
Am		450.8	402.7	343.5
Rc	267.1	267.2	268.5	265.2

[a] $^{av}\delta_{hf}^{pred1}$, $^{av}\delta_{hf}^{pred2}$, and $^{av}\delta_{hf}^{pred3}$ results are calculated using eq 9 with parameters for G($\mathbf{r}$), |V($\mathbf{r}$)|, and $\rho(\mathbf{r})$ in Table S37.

Finally, we investigated how changes in the cysteine side-chain conformation might be expected to influence the $C^{\beta}H_2$ hyperfine shifts. Using a Pc model system with the X-ray geometry (Figure S3A), we varied the H−C$^{\beta}$−S−Cu torsion angle, finding a Karplus type relationship[10,60] between δ_{hf} (or $\rho_{\alpha\beta}$) and θ (the H−C$^{\beta}$−S−Cu torsion angle), as shown in Figure S3B and Table S38. In the future, it may be possible to use these relationships, together with those discussed above, to help refine structure, particularly in the solid state, where Curie relaxation is absent.

Conclusion

The results that we have described above are of interest for a number of reasons. First, we report the results of a broad range

(60) Bertini, I.; Capozzi, F.; Luchinat, C.; Piccioli, M.; Vila, A. J. *J. Am. Chem. Soc.* **1994**, *116*, 651−660.

of quantum chemical calculations of the proton NMR hyperfine shifts in several BCPs: Am, Az, Pa, Pc, Sc, and Rc. The best results have a theory vs experiment correlation $R^2 = 0.94$, with a close-to-ideal slope = 1.01 and SD = 40.5 ppm, or 4.7% of the total experimental range of 862.5 ppm. Second, the computational results indicate that large structural models containing all weak axial ligands together with all hydrogen-bonded partners of all of the strong equatorial ligands, as well as geometry optimization, are needed to reproduce the experimental Cys−C^{β} proton NMR hyperfine shifts. Consequently, NMR hyperfine shifts are sensitive probes of large sections of active site structure in these systems. Third, we find an interesting effect of the hydrogen-bonded partners of the His ligands on the NMR hyperfine shifts that helps interpret some unique features of the different proteins. Fourth, we find that use of geometry-optimized structural parameters with an empirical shift prediction model leads to excellent predictions ($R^2 = 0.99$) of experimental Cys C^{β} proton NMR hyperfine shifts. Fifth, we carried out an AIM theory investigation, finding good correlations ($R^2 = 0.93-0.97$) between AIM properties at bond and ring critical points in the active site with the proton hyperfine shifts. Overall, these results are of general interest since they represent the first detailed quantum chemical investigations of ^{1}H NMR hyperfine shifts in BCPs that, when combined with other spectroscopic results, should be of use in structure refinement.

Acknowledgment. This work was supported in part by the U.S. Public Health Service (NIH Grant GM073216), the National Computational Science Alliance (Grant TG-MCB060084N), the Mississippi Center for Supercomputing Research, and an NSF EPSCoR award OIA-0556308. We also thank the reviewers for their helpful suggestions.

Supporting Information Available: Complete ref 21 and additional results (Tables S1−S38 and Figures S1−S3). This material is available free of charge via the Internet at http://pubs.acs.org.

JA075978B